

1 Sorption Phenomena In Transient Vapor Intrusion
2 Scenarios

3 Jonathan G. V. Ström^a, Shuai Xie^a, Eric M. Suuberg^a

4 *These authors contributed equally to this work*

5 ^a*Brown University, School of Engineering, Providence, RI, USA*

6 **Abstract**

Abstract here

7 *Keywords:* Vapor intrusion, Temporal variability, Sorption, Attenuation
8 factor

9 **1. Introduction**

10 Many vapor intrusion (VI) contaminants has the capacity to sorb onto soil
11 and various common indoor materials, but the role and more importantly,
12 the consequences of these sorption processes in VI are poorly understood[1,
13 2?]. The migration of contaminant vapors from its source into the VI
14 affected building and potential indoor sources are usually the prime concern
15 in VI investigations. Rarely is the sorbed contaminant vapors in the soil
16 or indoor considered in an investigation, but these may potentially act as a
17 capacitor, storing and releasing contaminant vapors in response to a change in
18 contaminant concentration. Consequently, contaminant vapors may be much
19 more persistent at a site that has undergone remediation, potentially reducing
20 the effectiveness of mitigation systems, or impeding site investigations.

21 It is well recognized that building materials has the capacity that sorb pol-
22 lutants. The sorptive capacity of various volatile organic compounds (VOCs)
23 of concern in VI have been tested on a variety of building materials, such
24 as density board[?], gypsum wallboard[?], and plywood and carpets[?
25]. However, most of these studies used relative high contaminant concen-
26 trations, usually around mg/m³[?] or even higher. This is several magni-
27 tudes higher than the concentrations relevant in VI and due to the non-linear
28 nature of sorption with respect to concentration, sorption studies at lower
29 concentration are needed.

Most of the VOC sorption studies have also focused on the interaction between building materials and formaldehyde[?], toluene, and decane[?]. However, one of the contaminants of greatest concern in VI - trichloroethylene (TCE), has not received likewise attention. This is despite the fact that sorbing TCE (and other VOCs) on activated carbon is extensively used to treat indoor air contaminant and their use with passive sorption tube samplers[3].

Over the years many VI sites have been investigated for their potential exposure risk. Most of these are conducted by private industries but a few notable academic ventures exist as well. Two well-known examples of these are the studies of "Sun Devil Manor" near Hill Air Force Base in Utah, and a building in Indianapolis, Indiana. Both of these sites were outfitted with a wide variety of instrumentation to investigate the VI drivers at these sites. These studies yielded some of the richest VI datasets available and gave invaluable insights, in particular in the application of CPM[4] and sub-slab depressurization (SSD) mitigation systems[5, 6]. However, neither of these studies considered the role of sorption had at these sites.

The potential impact of sorption may perhaps be most significant in the application of the controlled pressure method and various mitigation schemes. The controlled pressure method (CPM) is the forced over- and depressurization of a building to max- and minimize the contaminant entry to the building. This aids the investigator to ascertain the worst-case VI scenario and help identify potential indoor contaminant sources[7, 4]. However, if the building has a large capacity to sorb contaminant vapors onto various materials, these may be sorbed and desorbed in response to the changing condition, potentially preventing corresponding changes in indoor air contaminant concentrations. The same is true for various mitigation schemes, while they may successfully prevent contaminant vapors from entering the house, these may still be released from the interior over an unknown period of time[1, 2].

In the past VI models have been used to gain insight into VI when no field or experimental data has been available. Previously examples of VI modeling studies are the role of rainfall in VI[8], or drivers of temporal variability in some of the aforementioned sites[9]. However, while many VI models include a sorption term in the governing equation for contaminant transport in soils, none have explored the role of sorption in VI in a transient simulation. The reason for this is two-fold. First, there has been a general lack of interest in sorption and VI thus far. Secondly, the vast majority of VI modeling efforts

68 and studies has focused on steady-state analyses of VI, and sorption only
69 affects soil contaminant transport in time-dependent scenarios.

70 To bridge this knowledge gap we will begin to explore the role of sorp-
71 tion in VI through a combined effort of experimental and simulation work.
72 Sorption data of TCE on various common indoor materials and Applying soil
73 will be measured in a fixed bed sorption experiment. These sorption data
74 will then be incorporated into a three-dimensional finite element model of
75 VI. For this purpose we will consider a prototypical VI scenario where a free-
76 standing house with a basement is overlying a homogenously contaminated
77 groundwater source. Using this model we will investigate how the dynamic
78 contaminant transport is affected in general by sorption, how indoor sorp-
79 tion materials affect indoor air concentration as the building's pressurization
80 fluctuates and how indoor air concentration are affected by indoor materials
81 following successful mitigation of the structure.

82 2. Methods

83 2.1. Experimental Setup

84 The TCE dynamic sorption process of different building materials were
85 determined by use of a method schematically shown in Figure 1. This method
86 involved a selected material contained in an adsorption column through which
87 TCE-containing gas was passed, and subsequent thermal desorption and mea-
88 surement of the total amount of adsorption. During the adsorption part of
89 the process, stainless steel tubes were packed with building materials held in
90 place by glass wool. The amount of building material normally held in the
91 tube was around 1 g. It was determined that neither the glass wool nor the
92 stainless steel tube would retain significant amounts of TCE. The sample-
93 containing tubes were first exposed desired low concentrations of TCE in
94 nitrogen, which were then allowed to interact with the flow for varying pe-
95 riods of time. The typical flow rate of the nitrogen was 60 ml/min and the
96 concentrations of TCE was around 1.1 ppbv. All of these adsorption experi-
97 ments were conducted at room temperature. After a given time of exposure
98 to the TCE-containing flow, that flow was stopped, and the sample tube
99 was attached to a sorbent tube placed downstream of the sample tube. The
100 sample tube was arranged such that the direction of the nitrogen flow in
101 the subsequent desorption process was opposite that of the TCE-containing
102 nitrogen flow during the adsorption process. During the thermal desorption

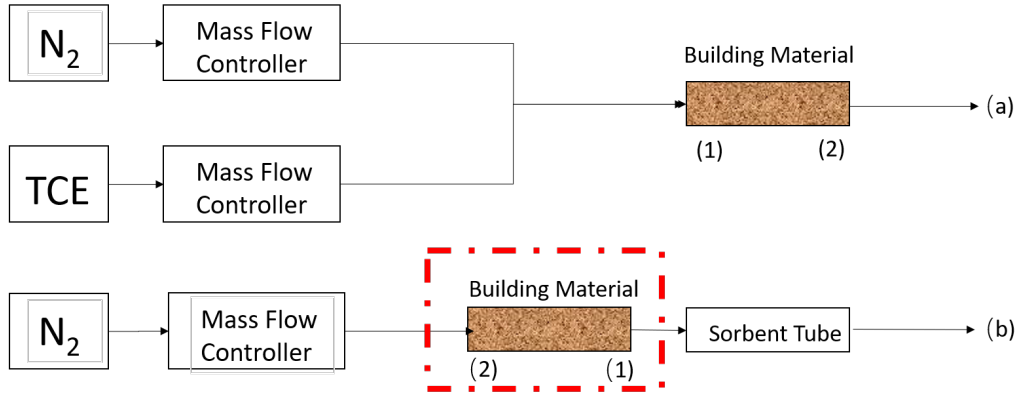


Figure 1: Schematic of experimental setup.

step, the sample containing tube was covered by a heating mantle which permitted its heating at 100 °C. This allowed fully desorbing the TCE which had been held on the sample into a pure nitrogen flow, which carried it to the room temperature downstream sorbent tube, where it was again fully adsorbed. These tubes fully capture all of the TCE desorbed, from the samples, and the amount of TCE was analyzed by Gas Chromatography (GC) with an Electron Capture Detector(ECD).

2.2. Numerical Model

To investigate the role of sorption in VI, we consider a simple VI scenario. Here we consider a house with a 10 by 10 m footprint, with the foundation bottom located 1 m below ground surface (bgs). The sole contaminant source is an uniformly TCE contaminated groundwater located 4 bgs, and the soil surrounding the house is assumed to homogenous and of a singular type. All contaminant vapors are assumed to enter the house through breaches in the foundation, modeled as a 1 cm wide crack that runs along the perimeter of the house. Finally we assume that sorption processes can occur both in the soil matrix and in the indoor environment (on various indoor materials).

Modeling this scenario requires us to simulate a couple of physics, many of which depend and interact with each other. The governing equations and the physics they govern are:

1. van Genuchten retention model - soil moisture.
2. Darcy's Law - air flow in the porous media.
3. Transport equation - contaminant transport in porous media.

Figure 2: The vapor intrusion model

126 4. Continuously stirred tank reactor (CSTR) - contaminant concentration
127 in the indoor environment.

128 These physics are implemented in COMSOL Multiphysics, a commercial
129 finite-element method package, which is used to solve our model. It is impor-
130 tant to note that the indoor environment is implicitly modeled, but instead
131 only given by the CSTR equation; the soil domain is explicitly modeled.

132 2.2.1. Vadose Zone Moisture Content

133 Since the contaminant transport occurs through three-phased the vadose
134 zone, it is important that we correctly account for soil moisture content and
135 its effect on advective and diffusive transport. In this modeled scenario, we
136 assume that the soil moisture is at steady-state and does not change, and
137 thus the soil moisture content is given by the retention model developed by
138 van Genuchten.

The van Genuchten retention model gives the soil water saturation as a function of elevation above groundwater. In turn this gives the water and gas filled porosities, and the relative permeability of the soil matrix.

$$Se = \begin{cases} \frac{1}{(1+\alpha z^n)^m} & z < 0 \\ 1 & z \geq 0 \end{cases} \quad (1)$$

$$\theta_w = \begin{cases} \theta_r + Se(\theta_s - \theta_r) & z < 0 \\ \theta_s & z \geq 0 \end{cases} \quad (2)$$

$$k_r = \begin{cases} Se^l [1 - (1 - Se^{\frac{1}{m}})]^2 & z < 0 \\ 0 & z \geq 0 \end{cases} \quad (3)$$

139 Se is the saturation, and ranges from 0 to 1, which represent completely un-
140 to fully saturated; z is the elevation above the groundwater in meters; θ_r ,
141 θ_s , θ_w , and θ_g are the residual moisture content, saturated porosity (or just
142 porosity), and water and air filled porosities respectively. All units are in
143 volume of phase divided by the volume of soil; k_r is the relative permeability
144 of water, which modifies the saturated permeability. This too ranges from 0
145 to 1, indicating completely im- and permeable respectively. $1 - k_r$ gives the
146 relative permeability of air.

147 *2.2.2. Gas Flow In The Vadose Zone*

148 The gas flow in the vadose zone is governed by a modified version of
 149 Darcy's Law. Originally, Darcy's Law was developed to describe flow in
 150 saturated porous media, but since we're interested in flow in unsaturated
 151 media, modification is necessary. An effective permeability that depends
 152 on the relative permeability from van Genuchten is introduced to allow for
 153 correct flow profiles in unsaturated porous media.

154 The vapor flow governing equation is given by

$$\frac{\partial}{\partial t}(\rho\theta_s) + \nabla \cdot \rho \left(- \frac{(1 - k_r)\kappa}{\mu} \nabla p \right) = 0 \quad (4)$$

155 Here ρ is the fluid density; ∇ is the del operator; κ is the saturated per-
 156 meability; μ is the fluid viscosity; and p is the fluid pressure. We assume
 157 that the contaminant vapors are so dilute that the gas flow properties can
 158 be taken to be those of air, and specifically at 20 °C and all the transport
 159 properties may be found in Table 1.

Boundary Conditions. To solve (4) we assign the atmosphere boundary (see
 Figure 2) to be at reference pressure and act as a gauge, i.e. zero pressure.
 The foundation crack boundary is assigned the indoor-outdoor pressure dif-
 ference value. Remaining boundaries are no-flow boundary conditions.

$$\text{Atmosphere} \quad p = 0 \text{ (Pa)} \quad (5)$$

$$\text{Foundation crack} \quad p = p_{\text{in/out}} \text{ (Pa)} \quad (6)$$

$$\text{All other} \quad -\vec{n} \cdot \rho_{\text{air}} \vec{u} = 0 \text{ (kg/(m}^2 \cdot \text{s))} \quad (7)$$

160 Here \vec{n} and \vec{u} are the boundary normal and gas velocity vectors.

161 *Initial Conditions.* For steady-state problems, the initial conditions don't
 162 matter, but is simply zero for the entire domain. When solving transient,
 163 the initial conditions are given by the steady-state solution.

164 *2.2.3. Mass Transport In The Vadose Zone*

165 Contaminants in the vadose zone exist in three phases - gaseous, solved in
 166 water, and sorbed onto soil particles. While there are three distinct phases,
 167 the water and gas phases are related via Henry's Law (8).

$$c_g = K_H c_w \quad (8)$$

Where c_g and c_w are the gas and water phase concentrations respectively in mol/m³; K_H is the dimensionless Henry's Law constant.

In this work, we consider sorption between the soil and vapor phases, as a function of the water contaminant concentration, through linear sorption (9).

$$c_s = K_{\text{ads}} \rho_b c_g = K_{\text{ads}} \frac{\rho}{1 - \theta_t} K_H c_w \quad (9)$$

Here the c_s is the solid phase concentration in mol/kg; ρ_b is the bulk density of the soil kg/m³, which is given by the density ρ and the total soil porosity θ_t ; K_{ads} is the sorption isotherm in m³/kg. Using Henry's Law and the linear isotherm we can express the total contaminant concentration in terms of the water contaminant concentration.

Mass transport in the vadose zone is governed by diffusion and advection and is given by (10).

$$R \frac{\partial c}{\partial t} = \nabla \cdot [D_{\text{eff}} \nabla c] - K_H \vec{u} \cdot \nabla c \quad (10)$$

The first term in (10) gives the change in contaminant water concentration with respect to time, modified by the *retardation factor*, R , which is discussed below; The second is the effective diffusive flux which is modified by the effective diffusion coefficient D_{eff} which is also discussed below. The third is the advective flux where \vec{u} is the soil-gas velocity from Darcy's Law, which when multiplied with K_H gives the gas phase concentration advective flux.

Contaminant entry into the building. The contaminant enters the building through a combination of advection and diffusive fluxes and is given by (11).

$$j_{ck} = \begin{cases} u_{ck} c_g - \frac{D_{\text{air}}}{L_{\text{slab}}} (c_{in} - c_g) & u_{ck} \geq 0 \\ u_{ck} c_{in} - \frac{D_{\text{air}}}{L_{\text{slab}}} (c_{in} - c_g) & u_{ck} < 0 \end{cases} \quad (11)$$

Here the j_{ck} is the molar contaminant flux into the building in mol/(m² · s); D_{air} is the contaminant diffusion coefficient in pure air in m²/s; L_{slab} is the thickness of the foundation slab in m. The flux expression changes if there is a bulk flow into the building, i.e. $u_{ck} \geq 0$, or out of the building.

Retardation factor. As the contaminants are transported through the vadose zone, the partitioning between the various phases increases the contaminant

194 residency time, retarding the transport of contaminants. This effect is rep-
 195 resented by R which is the retardation factor (12).

$$R = \theta_w + \theta_g K_H + \rho_b K_H K_{\text{ads}} \quad (12)$$

Here θ_w , θ_g are the water and gas filled soil porosities; K_{ads} is the solid-gas phase sorption isotherm in m^3/kg . The diffusive and advective transport retardation is proportional to the inverse of R .

$$D_{\text{retarded}} = \frac{D_{\text{eff}}}{R} \quad (13)$$

$$\vec{u}_{\text{retarded}} = \frac{\vec{u}}{R} \quad (14)$$

196 It should be noted that the soil-gas velocity, \vec{u} , is not retarded in of itself,
 197 but rather just the contaminant being transported through advection, giving
 198 a effective bulk velocity.

199 *Effective diffusivity.* The effective diffusivity in the vadose zone varies with
 200 the soil moisture content, from being close to that in water when fully sat-
 201 urated and vice versa. Millington-Quirk developed (15) which describes the
 202 effective diffusivity in variably saturated porous media.

$$D_{\text{eff}} = D_{\text{water}} \frac{\theta_w^{\frac{7}{3}}}{\theta_t^2} + \frac{D_{\text{air}}}{K_H} \frac{\theta_g^{\frac{7}{3}}}{\theta_t^2} \quad (15)$$

203 Where the porosity fractions are the water and gas phase tortuosity terms;
 204 D_{air} and D_{water} are the contaminant diffusion coefficient in air and water
 205 respectively in m^2/s .

Boundary Conditions. A few boundary conditions are required to solve (10). In this model, the sole contaminant source is assumed to be the homogenously contaminated groundwater, which we assume to have a fixed concentration. The atmosphere acts as a contaminant sink, and any contaminant that makes it to this boundary is infinitely diluted, thus this is simply a zero concentration boundary condition. Contaminants leave the soil domain and enter the building through a combination of advective and diffusive gas phase transport. The last boundary condition is applied to all other boundaries and is

a no-flow boundary.

$$\text{Groundwater} \quad c_w = 0 \text{ (mol/m}^3\text{)} \quad (16)$$

$$\text{Atmosphere} \quad c_w = c_{gw} \text{ (mol/m}^3\text{)} \quad (17)$$

$$\text{Foundation crack} \quad -\vec{n} \cdot \vec{N} = -\frac{j_{ck}}{K_H} \text{ (mol/(m}^2 \cdot \text{s))} \quad (18)$$

$$\text{All other} \quad -\vec{n} \cdot \vec{N} = 0 \text{ (mol/(m}^2 \cdot \text{s))} \quad (19)$$

$\vec{n} \cdot \vec{N}$ is the dot product between the boundary normal vector and the contaminant flux; j_{ck} is the contaminant vapor flux into the building. We assume that only contaminants in the gas phase enter the building, and dividing j_{ck} by K_H we get proper accounting in terms of the water phase concentration.

Initial Conditions. For a steady-state condition the initial conditions don't matter, but are set to be zero everywhere. For transient simulations in this work, the steady-state solution is always used as an initial condition.

2.2.4. Indoor Environment

The indoor air space is modeled as a continuously stirred tank reactor (CSTR) given by (20). Contaminants are assumed to only enter through the foundation crack, represented by n_{ck} , which is calculated by integrating the contaminant flux over the foundation crack boundary. The product of air exchange rate, which govern how many house volumes are exchanged with the outside per time unit, and indoor air contaminant concentration gives the contaminant exit rate. The sorption of contaminant is given by the sorption reaction term in (22) and the sorbed contaminant concentration is given by (21).

$$V_{\text{bldg}} \frac{\partial c_{\text{in}}}{\partial t} = n_{\text{ck}} - A_e c_{\text{in}} V_{\text{bldg}} + r_{\text{sorb}} V_{\text{mat}} \quad (20)$$

$$V_{\text{mat}} \frac{\partial c_{\text{sorb}}}{\partial t} = -r_{\text{sorb}} V_{\text{mat}} \quad (21)$$

$$r_{\text{sorb}} = k_1 c_{\text{sorb}} - k_2 c_{\text{in}} \quad (22)$$

$$n_{\text{ck}} = \int_{A_{ck}} j_{ck} dA \quad (23)$$

Here V_{bldg} and V_{mat} are the indoor control volume and volume of indoor material in m^3 ; c_{in} and c_{sorb} are the indoor and sorbed (onto the indoor

Table 1: Transport properties and model parameters

material) contaminant concentrations in mol/m^3 ; n_{entry} is the contaminant entry rate in mol/s , which is calculated by integrating the contaminant flux j_{ck} over the foundation crack area; r_{sorb} sorption rate in $\text{mol}/(\text{m}^3 \cdot \text{s})$; k_1 and k_2 are desorption and sorption reaction constants in $1/\text{s}$.

Fitting Kinetic Parameters. To calculate the indoor sorption rate we need k_1 and k_2 . These values are found by solving (22) numerically and then finding the best k_1 and k_2 by fitting them to the experimental data via least square. We use Runge-Kutta method of order 5(4) as the numerical solve, which is implemented together with the least square method in the SciPy python package[10].

3. Results & Discussion

3.1. Fitting Sorption Parameters

Using the numerical fitting scheme described in section 2.2.4 with the sorption data from the method described in section 2.1, the kinetic sorption parameters k_1 and k_2 are fitted. Figure 3 shows the result of this fitting and the sorption data for three select materials - wood, Appling soil, and cinderblock concrete. The k_1 and k_2 represent the rate at which TCE desorbs and sorbs respectively onto/from the material of interest. The equilibrium sorption constant is, using the formulation in (22), given by

$$K = \frac{k_1}{k_2} \quad (24)$$

and is used as the sorption isotherm. Here a small K indicate that there is a greater propensity for contaminant sorption.

To use the soil sorption isotherm in (10) K needs to be converted from being unitless to m^3/kg . This is done by multiplying the inverse of K isotherm with inverse of the soil bulk density ρ_b , which is taken to be $1460 \text{ kg}/\text{m}^3$.

$$K_{\text{ads}} = \frac{1}{K\rho_b} = 5.28 \text{ (m}^3/\text{kg)} \quad (25)$$

Table 2 shows the fitted parameters for the tested materials. Based on this these results we can see that cinderblock and soil have orders of magnitude

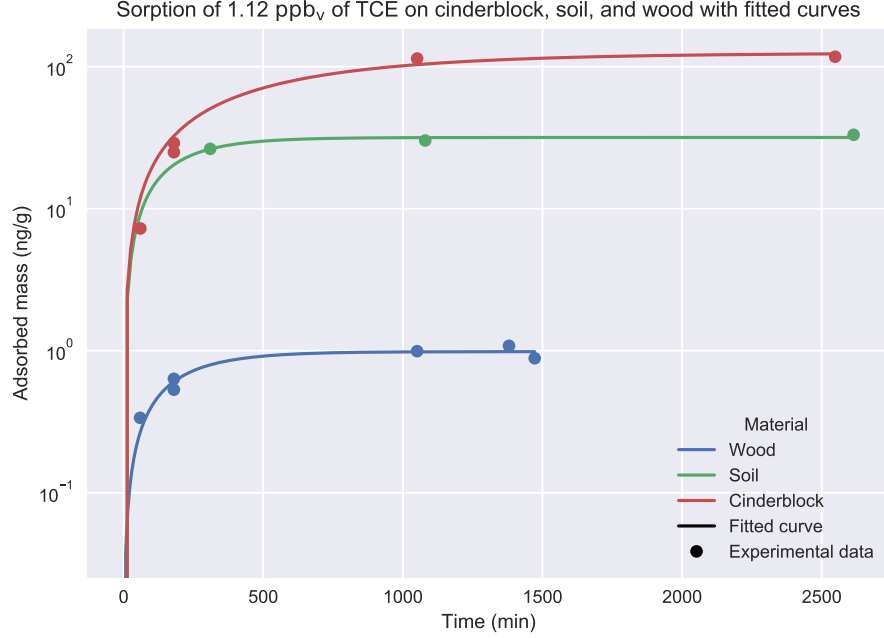


Figure 3: Experimental data of sorption of TCE onto three select materials as well as fitted sorption rates based on the kinetic model (22).

larger sorption capacities than wood or drywall does. We can also see by the k_2 values that soil and cinderblock sorb quickly, much faster than a material with similar sorptive capacity such as paper.

Table 2: Fitted kinetic sorption parameters based on sorption experiment data.

Material	k_1 (1/hr)	k_2 (1/hr)	K
Wood	0.32	44.90	$7.10 \cdot 10^{-3}$
Drywall	0.41	87.94	$4.65 \cdot 10^{-3}$
Carpet	0.26	58.74	$4.42 \cdot 10^{-3}$
Paper	0.04	88.37	$4.55 \cdot 10^{-4}$
Soil	0.34	2636.57	$1.30 \cdot 10^{-4}$
Cinderblock	0.10	4175.16	$2.40 \cdot 10^{-5}$

254 *3.2. Soil Sorption's Retarding Effect*

Building pressurization is a key factor in VI that influences the advective contaminant transport. The magnitude of change in response to a pressurization change is significantly influenced by a range of factors, such as soil permeability, foundation depth, or soil moisture. To demonstrate the effect that soil sorption has on contaminant soil mass transport in the VI context, we run two types transient simulation where initially the modeled structure is at a steady -5 Pa, i.e. slightly depressurized. At the start of the simulation, the building building is 1) further depressurized to -15 Pa, or 2) overpressurized to 15 Pa, and the simulation is allowed to run for 72 hours.

$$\text{Depressurization : } \Delta p_{\text{in/out}} = \begin{cases} -5, & t = 0 \text{ (hr)} \\ -15, & 0 < t \leq 72 \text{ (hr)} \end{cases} \quad (26)$$

$$\text{Overpressurization : } \Delta p_{\text{in/out}} = \begin{cases} -5, & t = 0 \text{ (hr)} \\ 15, & 0 < t \leq 72 \text{ (hr)} \end{cases} \quad (27)$$

255 For each of these cases, the simulation is run using two different soil types
 256 - sand and sandy loam. Sand is assumed here to not sorb any TCE, while
 257 for sandy loam a range of sorption isotherms are used. These range from
 258 no sorption ($K_{\text{ads}} = 0 \text{ (m}^3/\text{kg})$) to the experimentally determined sorption
 259 isotherm ($K_{\text{ads}} = 5.28 \text{ (m}^3/\text{kg})$) in intervals multiplicative by 10^{-2} . With the
 260 experimentally determined isotherm, we see that the ratio between sorbed
 261 concentration and soil-gas phase concentration is 7708, i.e. there is a much
 262 larger amount of sorbed contaminant. When $K_{\text{ads}} = 5.28 \cdot 10^{-4} \text{ (m}^3/\text{kg})$ this
 263 ratio is roughly unity (0.77), which is good to keep in mind in the following
 264 discussion. These ranges of values can be used both to represent a soil that
 265 has a smaller sorptive capacity or a situation where the sorbed and gas phase
 266 has not quite reached equilibrium.

267 In the top panel of Figure 4, the indoor air contaminant concentration
 268 as the simulated building is undergoing the pressurization in (26) case. Here
 269 we can see that for the case when the surrounding soil consists of sand, the
 270 indoor concentration increases rapidly as the building is further pressurized.
 271 The rate of increase decreases significantly for the sandy loam cases, and
 272 progressively retards are the sorbed mass increases (K_{ads} increases).

273 The bottom left panel shows how far away the indoor air concentration (as
 274 attenuation factor) for each case is from reaching equilibrium. At the start
 275 of the simulation, the building starts with an attenuation of α_0 , which is the

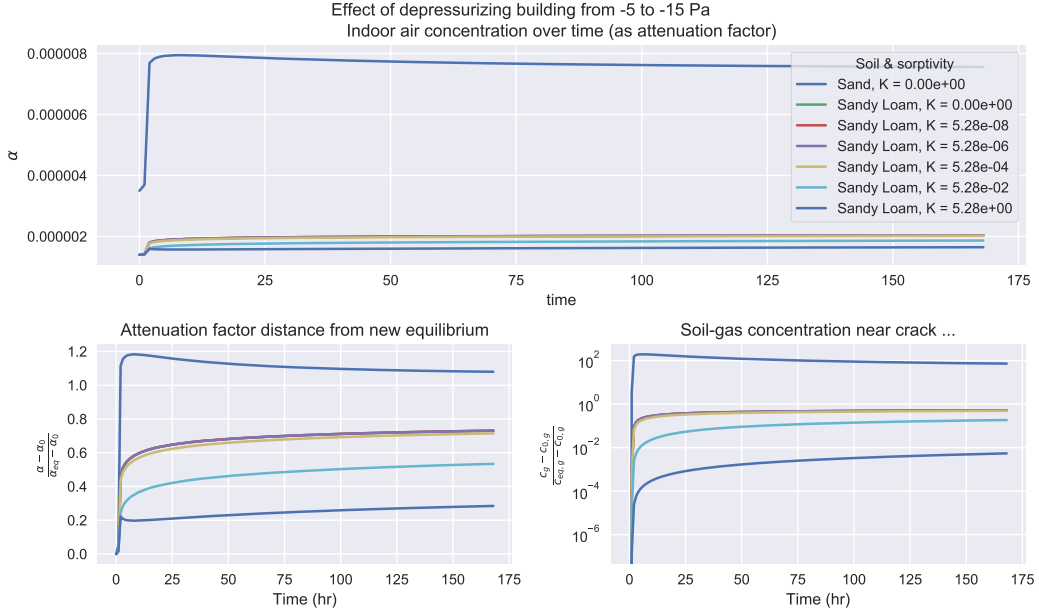


Figure 4

276 steady-state concentration when the building is pressurized with -5 Pa. As
 277 the building is further depressurized to -15 Pa, the indoor air concentration
 278 will approach a new equilibrium state α_{eq} (the result of which is from a
 279 steady-state simulation at that pressurization). By plotting $\frac{|\alpha - \alpha_0|}{|\alpha_{eq} - \alpha_0|}$ we can
 280 easily see how far away we are from the new equilibrium state, and a value
 281 of 0 represents that we are at the initial concentration, i.e. $\alpha = \alpha_0$, and a
 282 value of 1 represents $\alpha = \alpha_{eq}$.

283 This sort of analysis is applied to the bottom right panel as well, but
 284 instead of the indoor air concentration (as attenuation factor), we consider
 285 the average soil-gas concentration in a 5 cm diameter cylinder that envelop
 286 the entire perimeter crack. The choice of 5 cm is arbitrary, but helps illustrate
 287 what happens with the near-foundation-crack soil-gas concentration, changes
 288 in which allow us to better understand how the contaminant is transported
 289 into the building from the soil. The same could be done for the soil-gas
 290 velocity of course, but the rate of soil-gas velocity change is virtually the
 291 same for all of these cases, and reaches the new equilibrium velocity very
 292 quickly (much faster than the concentration) and is thus omitted from the
 293 figure.

Before discussing the role of sorption here, we can first compare the non-sorbing sand and sandy loam cases. Due to the higher permeability and lower moisture content, sand is significantly more permeable to gas flow than sandy loam (see Table 1 for permeability values). Consequently the advective transport through the foundation crack is much more significant, which is indicated by a Péclet number of around 4 versus 0.2 at a -15 Pa pressurization for sand and sandy loam respectively.

Due to the advection dominated transport mechanism in the sand case, the indoor air concentrations are temporarily elevated above the equilibrium concentration at -15 Pa, while the soil-gas concentration moves further away from equilibrium. (Note that the absolute distance from equilibrium is plotted in Figure 4 which is why at first glance one might think that the soil-gas concentration is two order of magnitude higher initially, but actually is two order of magnitude lower.) This phenomena occurs because initially more contaminants are drawn into the building from the near crack area than can be resupplied, temporarily depleting the local soil-gas contaminant concentration.

One can notice that many of the sandy loam lines overlap, and start diverging from each other when $K_{\text{ads}} = 5.28 \cdot 10^{-4}$ (m^3/kg), at the point where the ratio of sorbed and soil-gas concentration are roughly equal. We see that this divergence occurs simultaneously in the indoor air and soil-gas contaminant concentration. However, since the indoor air concentration depend on the soil-gas concentration, we know that this is where the relevant difference is.

The simple reason for this is that it is at this threshold the sorptive contribution to the retardation factor (12) starts to becomes larger than the other terms.

$$\rho_b K_H K_{\text{ads}} > \theta_w + \theta_g K_H \quad (28)$$

Thus it is at this point that the contaminant transport in the soil starts to become retarded by sorption. The physical reason for this is that the partitioning between the various phases gives a residence time as the contaminant is transported. Under VI conditions, the values of $\theta_w + \theta_g K_H$ are bounded to relatively small values, while K_{ads} can vary by orders of magnitude, making sorption potentially a very significant retarder for soil transport.

Figure 5 shows the same sort of analysis as in Figure 4 but with the building pressurization following (27). The results here are more or less the same, with the notable exception that in the sand case, the final equilibrium

330 concentration is not initially exceeded. As the building is overpressurized,
 331 the indoor contaminant are pushed out into the soil. Since the indoor air con-
 332 centration is lower than the soil-gas concentration, this is entirely expected.

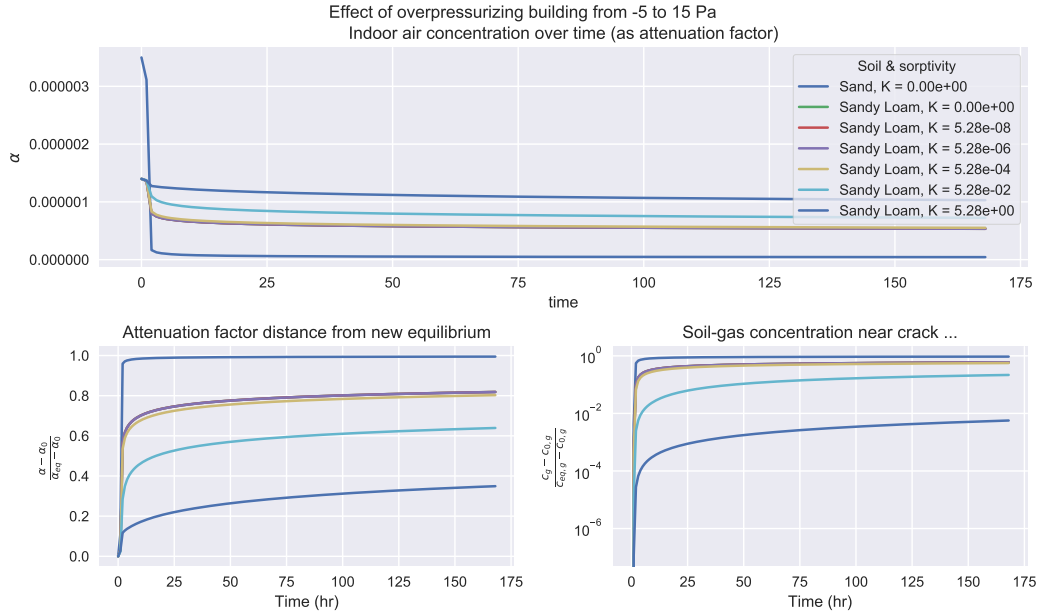


Figure 5

333 3.3. Indoor Material Sorption And Dynamics

334 We have now explored the effect that sorption has on contaminant mass
 335 transport in the sub-surface soil and seen its retarding effect. Now we turn
 336 to exploring the effect of sorption onto/from various indoor materials has on
 337 the indoor air contaminant concentration. (Here we assume that there is no
 338 soil sorption.)

339 To study this we consider the basement (the indoor air space) and assume
 340 that the inside surfaces are entirely made up of one of the materials we studied
 341 in 3.1. We also assume that the material covering the indoor surfaces has
 342 a certain thickness or depth that the contaminants can penetrate - giving
 343 a certain volume or mass of sorbing material in the indoor. Table 3 shows
 344 the surface area, penetration depth, and volume of each material studied.
 345 While obviously some of these rooms are non-conventional and arbitrarily
 346 designed, i.e. you're unlikely to find a room with carpeted walls, floors, and

ceiling, they do present some limiting cases of the potential effect of sorption onto/from these materials.

Material	d_p (mm)	V_{mat} (m ³)
Cinderblock	5	1.6
Wood	1	0.32
Drywall	10	3.2
Carpet	10	3.2
Paper	0.1	0.032

Table 3: The assumed contaminant penetration depth and subsequent volume of the sorbing indoor materials. The material surface area is assumed to be the same, and each material completely cover the surfaces of a 10x10x3 meter room.

The modeled building then undergoes a pressurization cycle, where at start of the simulation it is depressurized at -5 Pa and at steady-state. The building is then sequentially depressurized to -15 Pa, then pressurized to 15 Pa, and finally again depressurized to -5 Pa. For each sequence, the new pressurization is maintained for 24 hours. This pressurization cycle may be seen in the top left panel of 6. The choice of pressurization cycle is somewhat arbitrary, but ours can be used to represent limiting cases of natural pressurization variation, or artificially induced pressurization.

3.4. Indoor Material Sorption And Mitigation

4. Conclusions

Acknowledgements

This project was supported by grant ES-201502 from the Strategic Environmental Research and Development Program and Environmental Security Technology Certification Program (SERDP-ESTCP).

Declaration of interest: none

References

- [1] R. Meininghaus, L. Gunnarsen, H. N. Knudsen, Diffusion and Sorption of Volatile Organic Compounds in Building Materials-Impact on Indoor Air Quality, Environ. Sci. Technol. 34 (15) (2000) 3101–3108. doi:10.1021/es991291i.

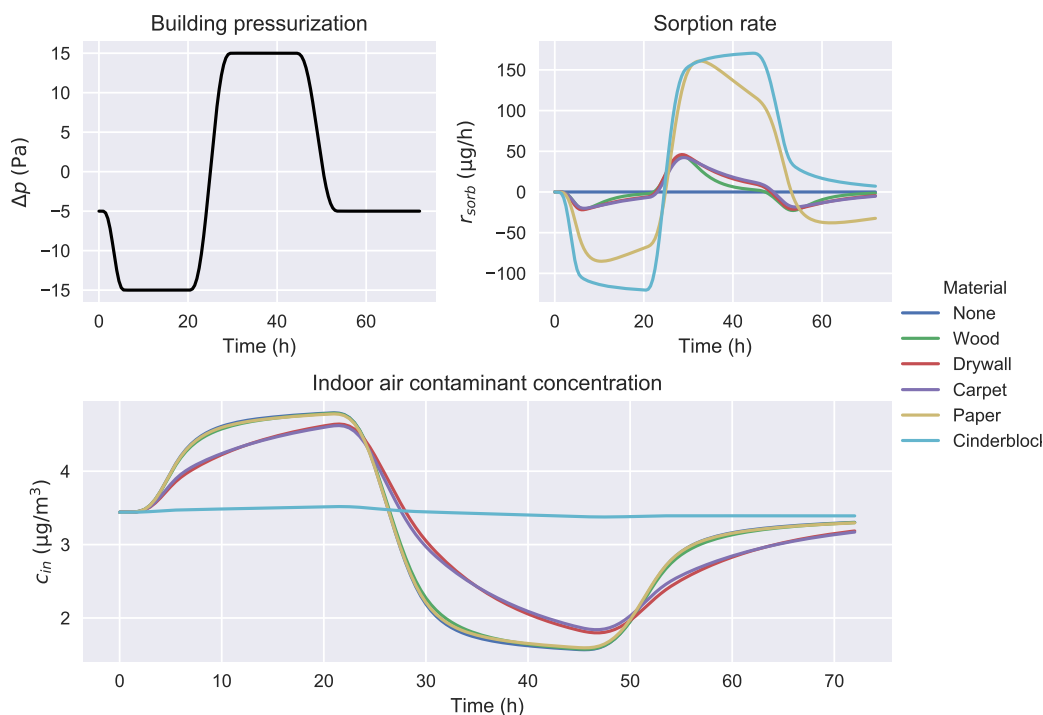


Figure 6: Comparison of how sorption onto/from various indoor materials affect the indoor air contaminant concentration (bottom) of a building that undergoes a pressurization cycle (top left). The rate of de- and sorption for each considered material during the cycle are also shown (top right).

- 369 [2] R. Meininghaus, E. Uhde, Diffusion studies of VOC mixtures in a building
370 material, *Indoor Air* 12 (4) (2002) 215–222. doi:10.1034/j.1600-
371 0668.2002.01131.x.
- 372 [3] U.S. Environmental Protection Agency, OSWER Technical Guide for
373 Assessing and Mitigating the Vapor Intrusion Pathway From Subsurface
374 Vapor Sources To Indoor Air (2015).
- 375 [4] C. Holton, Y. Guo, H. Luo, P. Dahlen, K. Gorder, E. Dettenmaier,
376 P. C. Johnson, Long-Term Evaluation of the Controlled Pressure Method
377 for Assessment of the Vapor Intrusion Pathway, *Environ. Sci. Technol.*
378 49 (4) (2015) 2091–2098. doi:10/f64j45.
- 379 [5] C. C. Lutes, R. S. Truesdale, B. W. Cosky, J. H. Zimmerman,
380 B. A. Schumacher, Comparing Vapor Intrusion Mitigation System

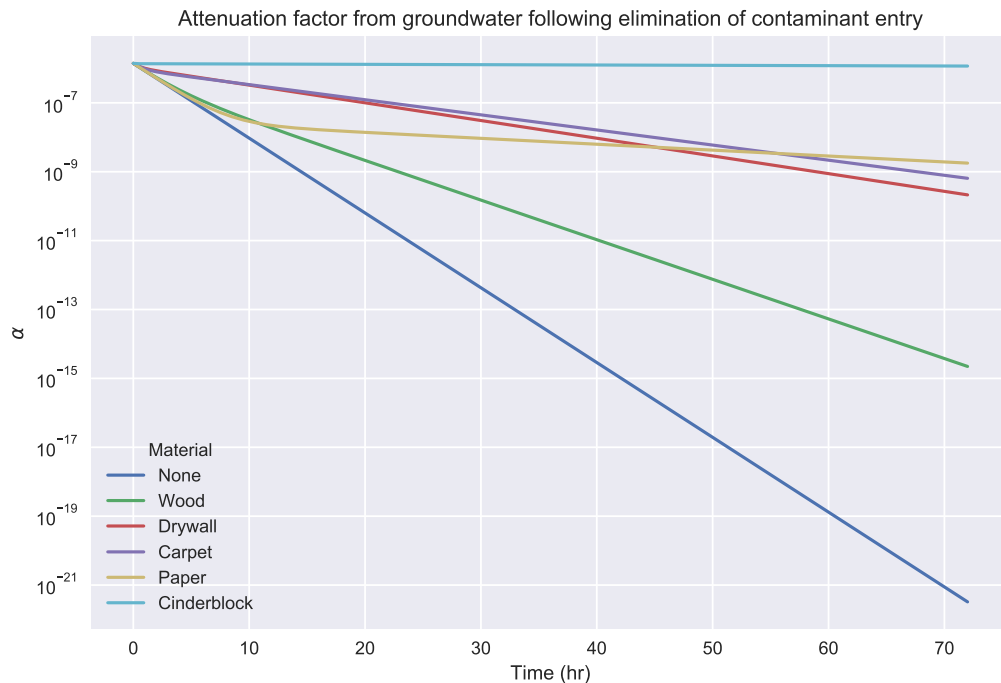


Figure 7

- 381 Performance for VOCs and Radon, Remediation 25 (4) (2015) 7–26.
 382 doi:10/gd6dfn.
- 383 [6] U.S. Environmental Protection Agency, Assessment of Mitigation Sys-
 384 tems on Vapor Intrusion: Temporal Trends, Attenuation Factors, and
 385 Contaminant Migration Routes under Mitigated And Non-mitigated
 386 Conditions (2015).
- 387 [7] T. McHugh, P. Loll, B. Eklund, Recent advances in vapor intrusion
 388 site investigations, Journal of Environmental Management 204 (2017)
 389 783–792. doi:10/gd6dgk.
- 390 [8] R. Shen, K. G. Pennell, E. M. Suuberg, A numerical investigation of
 391 vapor intrusion — The dynamic response of contaminant vapors to
 392 rainfall events, Science of The Total Environment 437 (2012) 110–120.
 393 doi:10/f4fp9s.
- 394 [9] J. G. V. Ström, Y. Guo, Y. Yao, E. M. Suuberg, Factors affect-

- 395 ing temporal variations in vapor intrusion-induced indoor air contam-
396 inant concentrations, Building and Environment 161 (2019) 106196.
397 doi:10.1016/j.buildenv.2019.106196.
- 398 [10] E. Jones, T. Oliphant, Pearu Peterson, SciPy: Open source scientific
399 tools for Python (2011).